Optimization of 4.7-keV X-ray titanium sources driven by 100-ps laser pulses

Xiong Jun(熊 俊)[a], Dong Jia-Qin(董佳钦)[a], Jia Guo(贾 果)[a,†], Wang Rui-Rong(王瑞荣)[a], Wang Wei(王 伟)[a], Fu Si-Zu(傅思祖)[b], and Zheng Wu-Di(郑无敌)[b]

[a] *Shanghai Institute of Laser Plasma, Chinese Academy of Sciences, Shanghai* 201800, *China*
[b] *Beijing Institute of Applied Physics and Computational Mathematics, Beijing* 100088, *China*

(Received 11 July 2012; revised manuscript received 8 November 2012)

An experiment with thin titanium foils irradiated by two pulses delayed in time is conducted on the Shenguang-II laser facility. A prepulse induces an underdense plasma, 2-ns later a main pulse ($\lambda_L = 0.35$ μm, $E_L \approx 120$ J, $\tau_L \approx 100$ ps) is injected into the underdense plasma and produces strong line emission from the titanium K shell (i.e., He_α at 4.7 keV). Data show that the intensity of 4.7-keV X-ray emission with the prepulse is approximately twice more than without the prepulse, and can be used as a backlighting source satisfying the diagnostic requirements for dense plasma probing. High-quality plasma images are obtained with the backlighting 4.7-keV X-rays in a Rayleigh–Taylor hydrodynamic instability experiment.

Keywords: X-ray source, prepulse, titanium foil

PACS: 52.38.Dx, 52.70.La **DOI:** 10.1088/1674-1056/22/6/065201

1. Introduction

Multi-keV X-ray sources are required as backlighting sources for diagnosing dense plasmas in inertial confinement fusion experiments, such as plasma hydrodynamic instability.[1–4] In these applications, the backlighting X-ray sources should have high brightness, high photo energy, and quasi-monochromatic spectrum. Multi-keV X-rays are emitted from the laser generated high-temperature plasma which has sufficient charge states and excitations. Generally, the high-temperature plasma is formed near the critical surface at a relatively low-density, and the peak emission region of multi-keV X-rays is from a high density region which must be conductively heated.

Multi-keV X-ray sources can be generated in the laser interactions with solid targets[5–7] and underdense gaseous targets.[8–12] Experiments have shown that the multi-keV X-ray conversion efficiencies (CEs) of underdense gaseous targets are about 10% of the laser energy, which is considerably higher than that of solid targets (0.1%–1%) due to good laser absorption of the gases. However, gas targets restrict spectral ranges, the Ar K-band is around 3-keV, theXe L-band around 4 keV and Kr K-band around 13 keV. To span a wider energy range, metal targets should be considered, although solid metallic targets exhibit much lower conversion efficiencies (CEs)[13] than underdense plasma sources. The production efficiencies of X-ray yield from solid targets have been studied each as a function of laser energy, wavelength, pulse length, and focusing properties in different experimental conditions.[14,15] In previous work of X-ray source optimization, Fournier *et al.*[16] used nanosecond laser beams to irradiate aerogel materials on the OMEGA laser, and Minoru Tanabe *et al.*[17] investigated multi-keV X-ray generation from low-density nanofiber-cotton targets composed of titanium dioxide. The CE of laser energy was enhanced 2 ∼ 3 times compared with that in the case of a foil target. Babonneau *et al.*[18] investigated the efficient multi-keV X-ray sources from laser-exploded metallic thin foils.

In order to enhance the CE of multi-keV X-ray emission from the solid target in our experiment, a prepulse is used to irradiate a solid target and generate the underdense plasma. After several nanoseconds, a main pulse interacts with the underdense plasma, thereby heating the underdense plasma to high temperature.

The measurements of X-ray emission from laser-heated titanium targets are presented in this paper. A weak prepulse irradiates a 5-μm thick foil target to produce the preformed plasma, and 2 ns later a main laser pulse ($\lambda_L = 0.35$ μm, $E_L \approx 120$ J, $\tau_L \approx 100$ ps) is delivered to heat the preformed plasma. The strong line emission from the Ti K-shell is produced. Data show that the intensity of 4.7-keV X-ray emission with the prepulse is approximately twice more than that without the prepulse. We use the enhanced X-rays as backlighting sources to diagnose a Rayleigh–Taylor hydrodynamic instability and then obtain high-quality plasma images.

2. Preliminary X-ray emission optimization by XRL-2D simulation code

A two-dimensional (2D) numerical XRL-2D code is used to design the experimental configuration. The XRL-2D code is a 2D non-equilibrium radiation hydrodynamics code with a

†Corresponding author. E-mail: jiaguo_2010@163.com

© 2013 Chinese Physical Society and IOP Publishing Ltd

diffusion approximation of radiation and the average atomic model. The flux-limited heat diffusion model is based on the Spitzer–Harm thermal conductivity, and the CE is evaluated with a flux limit value of $f = 0.1$. Therefore it only provides the total radiation energy, and cannot calculate the angular distribution of X-ray or radiation intensity of each K-shell line.

Generally, the main mechanism of the titanium K-shell emission production can be described by the collision-irradiative model. We focus on the H-like line and the He-like line of the titanium K-shell emission. H-like and He-like ions are excited by the hot electrons from the ground state to the first excited state ($n = 2$, with only one electron). Subsequently, the K-shell emission line is emitted by the spontaneous emission mechanism. Figure 1 shows the population distribution of H-like and He-like ions with different temperatures in steady-state with full radioactive escape. The electron temperature is above 2 keV and the electron density is above 10^{23} cm^{-3} in the optimal X-ray emission area. However, this condition cannot be satisfied because the laser energy is difficult to be coupled to the supercritical area.

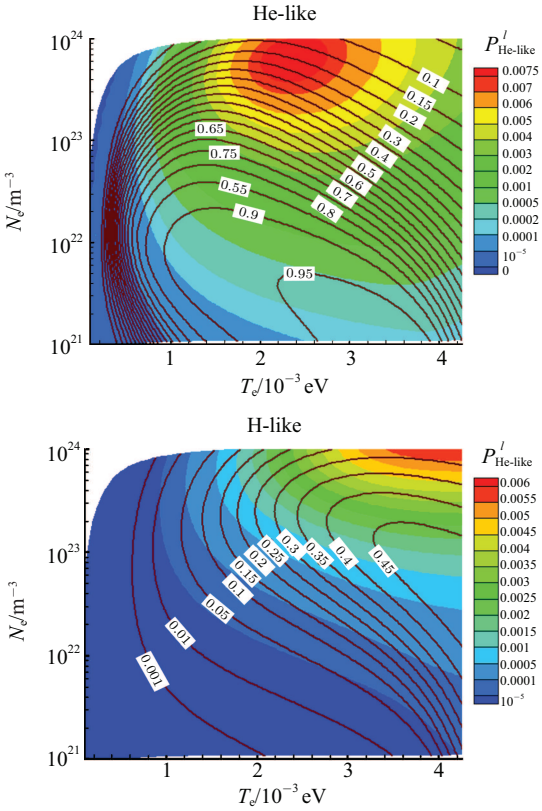


Fig. 1. (color online) Population distribution of K-shell ions in the N_e–T_e coordinate system (Contour lines show the ground state atomic population ($P^g_{\text{H-like}}$ and $P^g_{\text{He-like}}$). Colored areas show the first excited state population ($P^1_{\text{H-like}}$ and $P^1_{\text{He-like}}$)).

In the present model, the titanium plasma is an optically thin medium for the K-shell line emission. Thus, the actual population distribution of the ions is slightly different from the theoretical one. Based on numerical simulation, the preliminary optimal conditions are specified as follows. The electron density of the strong K-shell X-ray line ($n = 2$) emission region can be up to $N_e = 3 \times 10^{21}$ cm^{-3} $\sim 10^{22}$ cm^{-3}, and the optimum electron temperature should be above 2 keV. So we can estimate that the driven laser flux should be above 10^{15} W/cm^2.

3. Experimental setup at the Shenguang-II laser facility

The experiments are implemented in the Shenguang-II laser facility. Titanium foil targets are irradiated with up to four beams (each with 100-ps temporally Gaussian profile, $\lambda = 351$ nm) at an angular 45° from the target normal. The average energy per beam is about 30 J. Each laser beam consists of a prepulse and a main pulse. The interval between the prepulse and the main pulse (τ) is 2 ns and the intensity ratio of prepulse to the main pulse (η_{pre}) is changed from 0% to 20%. The four beams are focused onto titanium foil (thickness 5.0 ± 0.5 μm) targets through spherical lenses of f/3 at the same time. The intensity of the main pulse is fixed between 2×10^{15} W/cm^2–3×10^{15} W/cm^2 in a spot with a diameter of 200 μm.

The experimental setup is shown in Fig. 2. The diagnostic system includes a time-integrated pinhole camera (XPHC) and an X-ray elliptical crystal spectrometer.

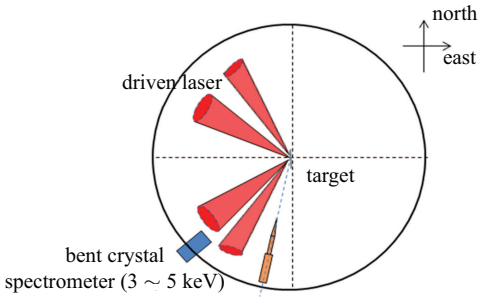


Fig. 2. (color online) Schematic setup of the experiment.

The X-ray emission volumes of targets are observed by a time-integrating pinhole camera. The pinhole camera is placed at an angle of 80° with respect to the normal direction of the target. The magnification is ten and the pinhole diameter is 10 μm. With a 50-μm titanium filter, the camera only provides an emitting zone size above 4 keV.

The X-ray elliptical crystal spectrometer is a high-resolution spectrometer that gives the time integrated X-ray spectrum with a spectral bandwidth depending on the crystal. A bent quartz crystal ($2d = 0.67$ nm) is installed in the spectrometer. The bent crystal spectrometer offers a spectral bandwidth between 3 keV and 5 keV. The detector medium is image plate (Fujifilm BAS-SR2025).[19] The crystal spectrometer can obtain the titanium K-shell lines with a 20-μm-thick

titanium filter, which provides a quasi-monochromatic X-ray source with the photon energy at approximately 4.7 keV.

4. Results and discussion

The results obtained for the titanium show an important increase of the multi-keV X-ray production by a factor from two to three, according to the prepulse. We also use the XRL-2D code to simulate the experiments, and compare the results with the experimental results obtained from the Shenguang-II laser facility. From these results, we find the appropriate driven laser conditions of the multi-keV X-ray probe.

From the XRL-2D code, we can see X-ray emitting zones with different values of $\eta_{\rm pre}$ in Fig. 3. Note that $\eta_{\rm pre} = 0\%$ corresponds to the case without the prepulse. Laser absorption efficiency without prepulse is 58%, which is lower than that with the prepulse (over 95%). Figure 3 clearly shows that when $\eta_{\rm pre}$ equals 0% the X-ray emission region expends to about 30 μm. It is significantly smaller than the X-ray emission region with the prepulse, which expends to almost 100 μm.

A large plasma expansion and a widening of the 4-keV emitting zones are visible for time-integrated X-ray pinhole camera when a prepusle is used. We present images of the above 4 keV radiating zones at 80° (Figs. 4(a) and 4(b)). The spot radius grows from 65 μm–75 μm without the prepulse to 90 μm–105 μm with the prepulse and the axial expansion (X-ray emission profile along the horizontal line) is from 50 μm–55 μm without the prepulse to 85 μm–90 μm with the prepulse (Figs. 4(c) and 4(d)). These images show the emitting spot enlargement, which is related to the plasma expansion. Due to the prepulse effect, the spot is widened 1.4 times and axially expanded 1.5 times. These images are in good coincidence with XRL-2D calculations.

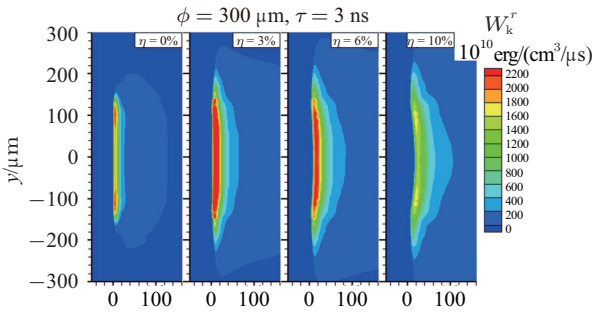


Fig. 3. (color online) X-ray emission region distributions at different values of $\eta_{\rm pre}$, 1 erg = 10^{-7} J.

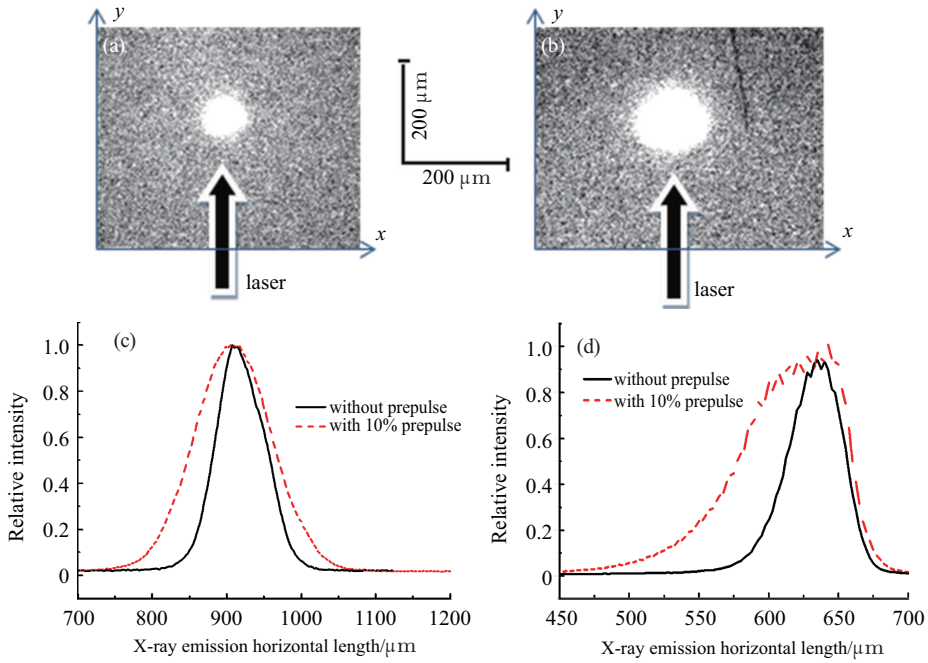


Fig. 4. (color online) Effects of a prepulse on above 4 keV X-ray emitting spots for 5-μm titanium foil in the cases: (a) without the prepulse and (b) with a prepulse of 10% main pulse intensity; (c) X-ray emission profiles (c) along the horizontal lines (the average of 15 pixels on the x axis, in the center of spot), and (d) along the vertical lines in panels (a) and (b) (the average of 15 pixels on the y axis, in the center of spot).

Figure 5(a) shows a measured time-integrated Ti K-shell X-ray spectrum from the foils. The Ti He-α line (0.261 nm and 0.262 nm) and Li-like line (0.263 nm) are obvious. X-rays below 4 keV and above 5 keV are absorbed by the titanium filter. The measured spectra of titanium with and without the prepulse are shown in Fig. 5(a). The solid line denotes the K-shell line of titanium with 10% intensity ratio prepulse, and the dotted line represents the line without the prepulse. The relative intensity of 4.7 keV (λ-0.26 nm) X-ray with the prepulse is approximately three times that without the prepulse.

Figure 5(b) shows the total energy of K-shell X-ray emissions in different values of $\eta_{\rm pre}$, calculated by XRL-2D. With the intensity of the prepulse increasing, the preformed plasma area created by the laser ablation becomes large, the electron temperature decreases. The total energy of the K-shell X-ray line radiation increases. When $\eta_{\rm pre}$ exceeds 10% and more, K-shell X-ray line radiation created by the prepulse increases rapidly, the total energy decreases on the contrary. According to the analysis of simulation, the optimal value of $\eta_{\rm pre}$ is 10% in the actual experimental backlight applications. With the prepulse turned on, the variation of the K-shell X-ray line radiation intensity is approximately 10% as the intensity of the prepulse changes.

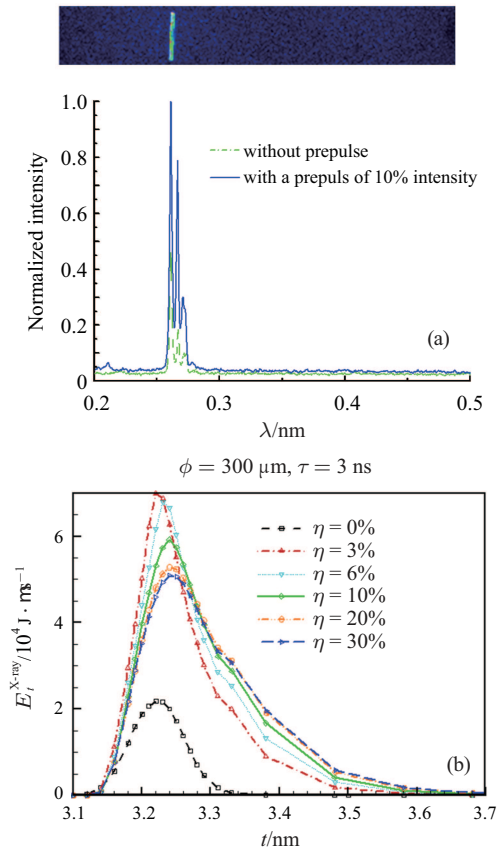


Fig. 5. (color online) K-shell line emissions in different conditions, showing (a) measured Ti K-shell X-ray time-integrated spectra (solid line) from the Ti foil in different $\eta_{\rm pre}$ values and (b) time evolutions of the K-shell X-ray obtained by the XRL-2D code at different laser irradiances, with the vertical axis representing X-ray energy per joule per microsecond.

K-shell X-ray line sources are studied each as a function of interval between the prepulse and the main pulse (τ). Figure 6 shows the energy of X-ray emission with different τ values. When τ increases, plasma length grows larger, electron temperature achieves a lower value, and the instantaneous power of the K-shell X-ray line radiation is reduced. However, when τ becomes lower, the plasma temperature cools down rapidly and the X-ray duration becomes narrower. Thus, the optimization result is $\tau = 2$ ns.

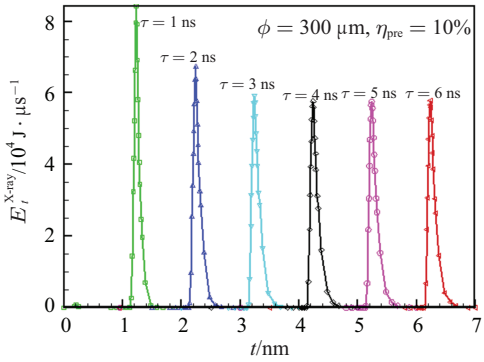
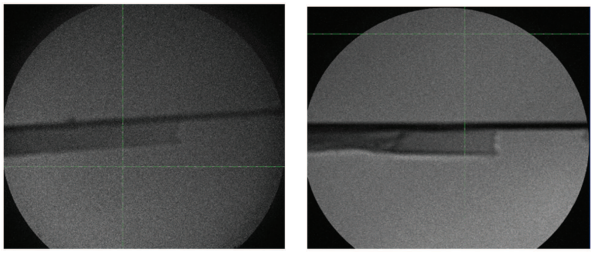


Fig. 6. (color online) K-shell line emissions at different values of τ ($\phi = 300$ μm, $\eta_{\rm pre} = 10\%$).

5. Application of X-ray backlight probe

We use the X-rays as a backlighting source to diagnose the static target by the pinhole projection method. Figure 7 shows that the quality of the image obtained by the optimized X-ray source (Fig. 7(b)) is better than that obtained before optimization (Fig. 7(a)). Figure 7 also shows that the 100-ps laser-driven X-ray backlight probe is significantly improved owing to the prepulse optimization. It can be used to diagnose the plasma in ICF experiments. Figure 8 shows high-quality 2D diagnostic images which are obtained by the optimized X-ray probe.



(a) Before optimization (b) After optimization

Fig. 7. Two diagnostic images from different X-ray sources obtained by the pinhole projection method: (a) before and (b) after optimization.

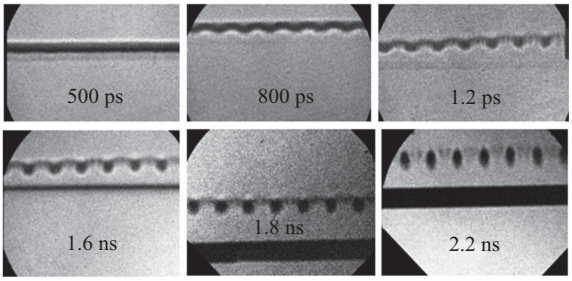


Fig. 8. Diagnostic images of the Rayleigh–Taylor hydrodynamic instability growth at different time moments.

6. Conclusions

To generate efficient X-ray sources for backlighting, multi-keV X-ray sources generated by heating titanium with 100-ps duration laser are investigated at the Shenguang-II laser

facility. With the experimental and theoretical analyses, we obtain the following conclusions.

Firstly, the simulation results suggest that the laser intensity should be higher than 10^{15} W/cm^2. The laser wavelength dependence stems from the greater ionization available at shorter wavelengths because of an increased density, wherein energy deposition occurs.

Secondly, the simulation shows that the total X-ray line emission is anisotropic. In the experiment, the intensity of the X-ray emission from the front target is significantly stronger than that from the rear target because of the presence of an X-ray emission absorption region near the high density cold plasma. The influence of the absorption region should be investigated by simulation and experiment in the future.

Thirdly, the experimental result shows that the intensity of 4.7-keV X-ray with a prepulse is approximately three times that without a prepulse. However, this value is almost ten according to the result of the XRL-2D simulation. The absorption efficiency of the laser and the K-shell X-ray line intensity may have been overestimated with such a high-intensity laser pulse ($> 10^{15}$ W/cm^2) because the nonlinear effects were not taken into account in our simulation.

Finally, the experimental data predict that optimal laser parameters ($\lambda_{\rm L} = 0.35$ μm, $I_{\rm L} > 10^{15}$ W/cm^2, $\eta_{\rm pre} = 10\%$, and $\tau = 2$ ns) are required for creating an efficient mutli-keV X-ray point source for diagnostic applications. We use a pinhole aperture as a point-projection backlighting source and obtain a variety of high-quality 2D plasma images in the ICF experiments.

Acknowledgment

We would like to thank the team of the Shenguang-II laser facility for their efforts.

References

[1] Woolsey N C, Riley D and Nardi E 1998 *Rev. Sci. Instrum.* **69** 418

[2] Ze F, Kania D R, Langer S H, Kornblum H, Kauffman R, Kilkenny J, Campbell E M and Tietbohl G 1989 *J. Appl. Phys.* **66** 1935

[3] Glendinning S G, Colvin J, Haan S, Kalantar D H, Landen O L, Marinak M M, Remington B A, Wallace R, Cherfils C, Dague N, Divol L, Galmiche D and Richard A L 2000 *Phys. Plasmas* **7** 2033

[4] Goldman S R, Caldwell S E, Wilke M D, Wilson D C, Barnes Cris W, Hsing W W, Delamater N D, Schappert G T, Grove J W, Lindman E L, Wallace J M, Weaver R P, Dunne A M, Edwards M J, Graham P and Thomas B R 1999 *Phys. Plasmas* **6** 3327

[5] Matthews D L, Campbell E M, Ceglio N M, Hermes G, Kauffman R, Koppel L, Lee R, Manes K, Rupert V, Slivinsky V W, Turner R and Ze F 1983 *J. Appl. Phys.* **54** 4260

[6] Phillion D W and Hailey C 1986 *Phys. Rev. A* **34** 4886

[7] Riley D, Woolsey N C and McSherry D 2002 *Plasma Sources Sci. Technol.* **11** 484

[8] Back C A, Grün J, Decker C, Suter L J, Davis J, Landen O L, Wallace R, Hsing W W, Laming J M, Feldman U, Miller M C and Wuest C 2001 *Phys. Rev. Lett.* **87** 275003

[9] Back C A, Davis J L, Grün J, Landen O L, Miller M C and Suter L J 2001 *Proc. SPIE* **4504** 133

[10] Back C A, Davis J, Grün J, Suter L J, Landen O L, Hsing W W and Miller M C 2003 *Phys. Plasmas* **10** 2047

[11] Fournier K B, Constantin C, Poco J, Miller M C, Back C A, Suter L J, Satcher J, Davis J and Grün J 2004 *Phys. Rev. Lett.* **92** 165005

[12] Fournier K B, Constantin C, Poco J, Miller M C, Back C A, Suter L J, Satcher J, Davis J F and Grün J 2004 *Proc. SPIE* **5196** 194

[13] Workman J and Kyrala G 2001 *Proc. SPIE* **4504** 168

[14] Kyrala G A, Fulton R D, Wahlin E K, Jones L A, Schappert G T, Cobble J A and Taylor A J 1992 *Appl. Phys. Lett.* **60** 2195

[15] Workman J and Kyrala G A 2001 *Rev. Sci. Instrum.* **72** 678

[16] Fournier K B, Constantin C, Poco J, Miller M C, Back C A, Suter L J, Satcher J, Davis J and Grun J 2004 *Phys. Rev. Lett.* **92** 165005

[17] Tanabe M, Nishimura H, Fujioka S, Nagai K, Yamamoto N, Gu Z Z, Pan C, Girard F, Primout M, Villette B, Brebion D, Fournier K B, Fujishima A and Mima K 2008 *Appl. Phys. Lett.* **93** 051505

[18] Babonneau D, Primout M, Girard F, Jadaud J P, Naudy M, Villette B, Depierreux S, Blancard C, Faussurier G, Fournier K B, Suter L, Kauffman R, Glenzer S, Miller M C, Grün J and Davis J 2008 *Phys. Plasmas* **15** 092702

[19] Tanaka, Yabuuchi T, Sato T, Kodama R, Kitagawa Y, Takahashi T, Ikeda T, Hinda Y and Okuda S 2005 *Rev. Sci. Instrum.* **76** 013507